

Article

Phenotypic Polymorphism in Two Endosymbiotic Bacteria of the Ciliate *Paramecium*: *Pseudolyticum multiflagellatum* and “*Ca. Megaira venefica*”

Ekaterina Kursacheva ^{1,†}, Alexander Korotaev ^{1,‡}, Konstantin Benken ², Natalia Lebedeva ³
and Elena Sabaneyeva ^{1,*}

¹ Department of Cytology and Histology, Faculty of Biology, Saint-Petersburg State University, 199034 Saint-Petersburg, Russia; ekatrusa@gmail.com (E.K.); alexander.korotaev@unibas.ch (A.K.)

² Core Facility Center for Microscopy and Microanalysis, Saint-Petersburg State University, 199034 Saint-Petersburg, Russia; cbenken@gmail.com

³ Core Facility Center for Cultivation of Microorganisms, Saint-Petersburg State University, 198504 Saint-Petersburg, Russia; nalebedeva@yandex.ru

* Correspondence: e.sabaneeva@spbu.ru

† Present address: Department of Plant and Environmental Sciences, Weizmann Institute of Science, Rehovot 7610001, Israel.

‡ Present address: Focal Area Infection Biology, Biozentrum, University of Basel, 4056 Basel, Switzerland.

Abstract: Here, we report a comprehensive description of the stable associations between two *Paramecium* species (*P. nephridiatum* and *P. caudatum*) and their cytoplasmic bacterial endosymbiont *Pseudolyticum multiflagellatum*. These spindle-like, rod-shaped, non-motile peritrichous bacteria demonstrate significant phenotypic polymorphism. Considering the differences in bacterial morphology and host species, several scientific groups have previously described these endosymbionts as distinct species. Our study provides brand-new molecular data, which allows us to unify earlier descriptions and determine the phylogenetic position of this endosymbiont as a member of the family “*Ca. Midichloriaceae*” (Rickettsiales). The distinguishing feature of this bacterium is the presence of a highly refractive granule in its cytoplasm, well detectable with differential interference contrast (DIC) microscopy. The protein nature of these peculiar inclusion bodies is considered. The other endosymbiont, “*Ca. Megaira venefica*”, co-inhabiting the cytoplasm of the studied *P. nephridiatum* strains, also displayed polymorphism, rounded forms being infected with phages.

Keywords: symbiosis; ciliates; *Paramecium*; Rickettsiales; *Ca. Midichloriaceae*; *Rickettsiaceae*; full-cycle rRNA approach; bacterial inclusion bodies; phage



Citation: Kursacheva, E.; Korotaev, A.; Benken, K.; Lebedeva, N.; Sabaneyeva, E. Phenotypic Polymorphism in Two Endosymbiotic Bacteria of the Ciliate *Paramecium*: *Pseudolyticum multiflagellatum* and “*Ca. Megaira venefica*”. *Diversity* **2023**, *15*, 924. <https://doi.org/10.3390/d15080924>

Academic Editor: Angelina Lo Giudice

Received: 17 July 2023

Revised: 3 August 2023

Accepted: 7 August 2023

Published: 11 August 2023



Copyright: © 2023 by the authors. Licensee MDPI, Basel, Switzerland. This article is an open access article distributed under the terms and conditions of the Creative Commons Attribution (CC BY) license (<https://creativecommons.org/licenses/by/4.0/>).

1. Introduction

Protists form a vast range of long and short-term symbiotic relationships with prokaryotes [1]. Among protists, ciliates, an extraordinarily widespread group inhabiting almost all aquatic environments, are especially prone to endosymbiosis [2]. Practically every cellular compartment of ciliated protists can be occupied by bacteria, leading to a drastic impact on ecology and the evolution of each partner of such relationships [3–6]. Historically, symbioses between *Paramecium* (Ciliophora) and bacteria have been extensively investigated due to the frequency and stability of such relations as well as to the ease of cultivation [7–10]. Over the last decades, the emergence of new methods of molecular research revived interest in *Paramecium*-bacteria symbiotic systems, enabling scientists to expand the descriptions of previously known endosymbionts with phylogenetic data, discover and define a plethora of new symbionts and study co-evolutionary genetic patterns and metabolic pathways of symbiotic interactions [11–17].

Most known bacterial symbionts of *Paramecium* belong to the orders Rickettsiales and Holosporales of the class Alphaproteobacteria [5,17,18]. Exceptions are few but

remarkable—for example, the R-body producing endosymbiont from the Gammaproteobacteria class (reviewed in [19]). The order Rickettsiales comprises four families to date: *Rickettsiaceae*, *Anaplasmataceae*, “*Candidatus* Midichloriaceae” and “*Candidatus* Deianiraeaceae” [13,16]. Representatives of each of these families, except *Anaplasmataceae*, have been found to be associated with *Paramecium*, being their ecto- or endosymbionts [13,18,20–23]. While the families *Rickettsiaceae* and *Anaplasmataceae* include several genera of Gram-negative intracellular pathogens of epidemiologic significance and thereby are thoroughly studied [24], “*Ca.* Midichloriaceae” is the most actively updated family of the order Rickettsiales, consisting so far exclusively of non-pathogenic symbiotic bacteria of different hosts: protists, arthropods and aquatic invertebrates [23].

In 1987, spindle-like endosymbiotic bacteria with peculiar refractive granules inhabiting the cytoplasm of *Paramecium caudatum* were discovered by Boss et al. [25]. These endosymbionts were morphologically described as Gram-negative rod-like non-motile bacteria, $2.0 \times 3.5\text{--}14.0 \mu\text{m}$ in size, with numerous flagella, individually surrounded by a symbiontophorous vacuole. Based on some morphological resemblance to bacteria of the genus *Lyticum*, these endosymbionts have been assigned to a novel species *Pseudolyticum multiflagellatum* within a novel genus *Pseudolyticum* [8,26]. Refractive granules detectible in the cytoplasm of most bacterial cells with differential interference contrast (DIC) appeared as large round electron-dense inclusion bodies in transmission electron microscopy (TEM) sections. They were tested with cytochemical techniques and defined as inclusion bodies of lipophilic nature.

In 1988, a complex symbiotic system consisting simultaneously of one macronuclear and two cytoplasmic endosymbiotic bacteria was described by Fokin in *Paramecium nephridiatum* [27], mistaken for *P. woodruffi* at that time [28]. One of those cytoplasmic bacteria had a similar morphology with *Ps. multiflagellatum*, but due to an overall smaller size has been assigned as a novel species—*Ps. minutus*.

The apparent morphological similarity of *Ps. multiflagellatum* and *Ps. minutus* casts doubt on whether these bacteria belonged to a distinct species. Both of these species were mentioned in the review of 2009 [29], while in the review published several years later the genus *Pseudolyticum* was considered to comprise one species only, *Ps. multiflagellatum*, inhabiting a single host—*P. caudatum* [30]. No molecular data were available at the time to determine its phylogenetic position.

Here, we report a comprehensive description of the endosymbionts morphologically similar to *Ps. multiflagellatum* and *Ps. minutus* found in *P. caudatum* [25] and *P. nephridiatum* [27], respectively. Based on molecular data and subsequent phylogenetic analysis, we revealed that *Ps. multiflagellatum* and *Ps. minutus* belong to one and the same species, *Ps. multiflagellatum*, demonstrating host-specific pleomorphism which might have obscured earlier descriptions.

The second discovered bacterium inhabiting the cytoplasm of *P. nephridiatum* strains belonged to the species “*Ca. Megaira venefica*” of the family *Rickettsiaceae*, a cosmopolitan endosymbiotic bacterium found to establish obligate associations with *Paramecium* [21]. A viral infection registered in a certain number of “*Ca. M. venefica*” cells was accompanied by changes in the size and shape of the bacteria resulting in the polymorphism of the population inhabiting one host cell.

2. Materials and Methods

2.1. Host Isolation, Cultivation and Identification

This study was performed on three *Paramecium* strains isolated from natural samples obtained throughout Russia: VL18-4, BMS16-3 and TRF-1 (Table 1). Ciliates were maintained at $+16\text{--}+22 \text{ }^\circ\text{C}$ in lettuce medium (salinity level: 0.0–5.0‰) inoculated with *Klebsiella aerogenes* [31]. Preliminary identification of ciliate species was carried out on the basis of their morphology [32] with a DM6000B microscope (Leica Microsystems GmbH, Wetzlar, Germany) equipped with differential interference contrast (DIC) and phase contrast, and then confirmed by molecular analysis.

Table 1. List of ciliate strains used in the study.

Strain Index	Host	Endosymbiont (s)	Sampling Sites	Cultivation Salinity Level (‰)
VL18-4	<i>P. caudatum</i>	<i>Ps. multiflagellatum</i>	Russia, Vladimir: pond (56.106928, 40.428814)	0
BMS16-3	<i>P. nephridiatum</i>	<i>Ps. multiflagellatum</i> , <i>Ca. M. venefica</i>	Russia, Karelsky region, Sredniy island: littoral pool (66.282500, 33.709444)	0
TRF-1	<i>P. nephridiatum</i>	<i>Ps. multiflagellatum</i> , <i>Ca. M. venefica</i>	Russia, St. Petersburg region, Peterhof: Troitsky stream (59.894074, 29.879725)	0–5.0
VL18-4 *	<i>P. caudatum</i>	No, aposymbiotic, spontaneous loss	Russia, Vladimir: pond (56.106928, 40.428814)	0
SD11-1	<i>P. nephridiatum</i>	No, naïve	Russia, St. Petersburg region, Sestroretsk: pond (60.096911, 29.958959)	0
Eta11-10	<i>P. nephridiatum</i>	No, naïve	Estonia, Tallinn, Kopli bay (59.4344225, 24.6766373)	5.0
1M15-3	<i>P. nephridiatum</i>	<i>Ca. M. venefica</i>	Russia, St. Petersburg region, Peterhof: ditch (59.878965, 29.851437)	0–5.0

* after the strain index marks the strain after the spontaneous loss of the endosymbionts.

2.2. DNA Extraction, PCR, Cloning and Sequencing

In order to minimize bacterial contamination, 100–150 starved cells of each ciliate strain were collected with a glass capillary and successively washed thrice in sterile distilled water, then fixed in 70% ethanol. Total genomic DNA was extracted using the NucleoSpin™ Plant II kit (Macherey-Nagel GmbH & Co., Düren, NRW, Germany) according to fungal DNA extraction protocol.

Amplification of the ciliate 18S rRNA gene was carried out using primers 18S_F9 (5'-CTGGTTGATCCTGCCAG-3') [33] and 18S_R1513Hypo (5'-TGATCCTTCYGCAGGTCC-3') [34]. Polymerase chain reactions (PCRs) were carried out using Encyclo DNA polymerase (Evrogen, Moscow, Russia) in a T100 thermocycler (Bio-Rad Laboratories, Inc., Hercules, CA, USA) running the following program: preliminary denaturation step at 94 °C for 3 min, then 35 cycles of denaturation at 94 °C for 30 s, annealing at 55 °C for 45 s and elongation at 72 °C for 90 s, then a final elongation step at 72 °C for 6 min. PCR products were directly sequenced in both directions using 18S rRNA gene internal primers: 18S_F783 (5'-GACGATCAGATACCGTC-3'), 18S_F919 (5'-ATTGACGGAAGGGCACC-3'), 18S_R536 (5'-CTGGAATTACCGCGGCTG-3') and 18S_R1052 (5'-AACTAAGAACGGCCATGCA-3') [35]. All sequencing reactions in this research were performed in the Core Facility Centre for Molecular and Cell technologies of St. Petersburg State University.

Amplification of the ciliate cytochrome c oxidase subunit 1 genes (COI) and subsequent direct sequencing of obtained PCR products were carried out using the primers F388dT (5'-TGTA AACGACGGCCAGTGGWKCBAAAGATGTWGC3') and R1184dT (5'-CAGGAAACAGCTATGACTADACYTCAGGGTGACCRAAAAATCA-3') [36]. PCRs were performed with Encyclo DNA polymerase (Evrogen, Russia). The temperature profile used was as follows: 94 °C–3 min, 35 cycles (94 °C–30 s, 56 °C–30 s, 72 °C–1 min), 72 °C–5 min.

Amplification of the endosymbiotic 16S rRNA gene was performed using primers 16S_αF19a (5'-CCTGGCTCAGAACGAACG-3'), 16S_R1522a (5'-GGAGGTGATCCAGCCGCA-3') [37] and DreamTaq polymerase (Thermo Fisher Scientific Inc., Waltham, MA, USA). Different temperature profiles were applied for 16S rRNA gene amplification depending on the host strain. “Touchdown” PCR [38] was performed with the DNA samples obtained from VL18-4 and BMS16-3 strains: 95 °C–3 min, 5 cycles (95 °C–30 s, 58 °C–30 s, 72 °C–2 min), 10 cycles (95 °C–30 s, 54 °C–30 s, 72 °C–2 min), 25 cycles (95 °C–30 s, 50 °C–30 s, 72 °C–2 min) and 72 °C–5 min. To amplify endosymbiotic 16S rRNA genes of the TRF-1 strain, a temperature profile identical to that used for the amplification of the 18S rRNA genes was used. PCR products were purified

with DNA Clean & Concentrator-5 kit (Zymo Research Corp., Irvine, CA, USA). Amplicons were ligated into the ptz57r/t vector and cloned with competent JM107 or JM109 *Escherichia coli* cells following the manufacturer's protocol of the InsTAclone PCR cloning kit (Thermo Fisher Scientific, Waltham, MA, USA). Sanger sequencing was performed with 10–30 clones obtained from each PCR product using vector-specific M13F/pUC and M13R/pUC primers and a set of 16S rRNA gene internal primers: 16S_F343ND (5'-TACGGGAGGCAGCAG-3'), 16S_F785ND (5'-GGATTAGATACCCTGGTA-3') and 16S_R515ND (5'-ACCGCGGCTGCTGGCAC-3') [37].

2.3. Fluorescence In Situ Hybridization (FISH) and Probe Design

An endosymbiont-specific probe (Pslyt1088, 5'-CTTTCGCTAGCAGTACCCT-3') was designed using the ARB 7.0 software package [39] and validated with SILVA TestProbe 3.0 [40] and RDP ProbeMatch (Release 11. Update 5) [41]. The probe sequence was deposited at probeBase [42].

Whole-cell FISH was carried out on Superfrost® Plus Gold slides (Thermo Fisher Scientific Inc., USA) strictly avoiding air-drying of the sample at any stage. Ciliate cells were fixed with 4% (*w/v*) paraformaldehyde (PFA) in phosphate-buffered saline (PBS) solution for 1 h at 4 °C. Then, basic protocol described in “whole-cell probing techniques” for Gram-negative bacteria [43] was applied except that ice-cold 70% methanol, not ethanol, was used at the next fixation step, and the dehydration step in the ethanol series was totally skipped. Hybridizations were performed by combining the specific probe Pslyt1088 with the bacterial probes: EUB338 (5'-GCTGCCTCCCGTAGGAGT-3') [44], 16S_MegVen1226 (5'-CCGAAGTGGATGCCTTTTGAG-3') [15], ALF1b (5'-CGTTTCG(C/T)TCTGAGCCAG-3') [45]. All probes were synthesized by Evrogen (Russia). Hybridization was carried out at 0%, 15% and 30% formamide concentrations for 1.5 h at 46 °C. Samples were afterwards washed twice with washing buffer for 30 min at 48 °C. Slides were then mounted in MOWIOL® 4-88 (Sigma-Aldrich Co. LLC, St. Louis, MO, USA), containing 0.1% PPD (Sigma-Aldrich Co. LLC, USA) and 300 nM DAPI (Sigma-Aldrich Co. LLC, USA). Slides were examined with a confocal laser scanning microscope TCS SPE (Leica Microsystems, GmbH, Wetzlar, Germany) at the Center for Microscopy and Microanalysis (CMM) of St. Petersburg State University, Russia.

2.4. Phylogenetic Analysis

The obtained 18S rRNA, COI and 16S rRNA gene sequences were examined using ChromasPro v 1.7.4 (Technelysium, South Brisbane, Australia) to evaluate and correct chromatograms. The sequences were subjected to a homology search in the NCBI nucleotide collection (nr/nt) database [46] using the BLAST service [47] for data pre-evaluation.

The newly obtained sequences and selected hits from BLASTn search results were aligned with Mafft [48], then curated with Gblocks [49]. Subsequent maximum likelihood (ML) phylogenetic analysis was performed with the IQ-TREE web server [50], providing automatic substitution model selection and combined branch support analysis with an ultrafast bootstrap [51] (min 1000 iterations), the SH-aLRT test [52] and aBayes test [53]. Visualization of the phylogenetic trees was performed with the Interactive Tree Of Life (iTOL) tool [54]; post-processing was made with BioRender [55] or Inkscape [56] if not specified.

2.5. Cytochemical Staining of Endosymbiotic Bacteria

Smear preparation. Approximately 5–10 ciliate cells, pre-starved for 24 h in sterile lettuce broth, were collected with a glass capillary in a small drop of medium and placed on a slide. The cells were then disrupted with a 26 G needle under a stereomicroscope control and air-dried. Air-dried smears were fixed with 8% paraformaldehyde (PFA) aqueous solution for 4 min at room temperature.

Amido Black 10B staining. Fixed smears were stained with Amido Black 10B (0.02%) in a mixture of 10% acetic acid and 90% methanol for 1 min. Smears were washed once with a mixture of 1% acetic acid and 70% ethanol prior to air-drying, embedding and examination [57].

Eosin staining. Fixed smears were stained with a mixture of equal volumes of 1% aqueous solutions of Y and B eosins and 1% Y eosin in alcohol (1:1), acidified with glacial acetic acid. The slide was rinsed once with water prior to air-drying, embedding and examination.

Congo Red staining. Fixed smears were stained with 0.25% Congo Red aqueous solution for 20 min, then washed once with water prior to air-drying, embedding and examination [58].

Sudan Black B staining. Fixed smears were stained with 0.3% Sudan Black B solution in 70% ethanol for 10 min, followed by a 1 s rinse with xylol prior to air-drying, embedding and examination. Bacteria with the inclusion bodies were easily detected with DIC, so no counterstaining was performed [59].

Embedding and examination. Stained smears were mounted in MOWIOL[®] 4-88 (Sigma-Aldrich Co. LLC, USA) prior to examination with DM6000B microscope (Leica Microsystems GmbH, Wetzlar, Germany) in bright field mode.

2.6. Transmission Electron Microscopy (TEM)

Ciliates were processed for electron microscopy as described by Szokoli et al. [20]. Briefly, the cells were fixed in a mixture of 1.6% aqueous paraformaldehyde (PFA) and 2.5% glutaraldehyde in 0.1 M phosphate buffer (pH 7.2–7.4) for 1.5 h at room temperature. Then, the cells were washed twice with the 12.5% sucrose solution in the phosphate buffer for 30 min and postfixed with 1.6% osmium tetroxide for 1 h at 4 °C. The cells were successively dehydrated in an ethanol series, ethanol/acetone mixture (1:1), 100% acetone and were gradually mounted into the embedding medium prepared according to the manufacturer's protocol from the SPI-PON[™] 812 KIT (Structure Probe, Inc., West Chester, PA, USA). After each step of fixation, dehydration and embedding cells were pelleted by centrifugation at 240–660 rcf for 3–6 min. The resin polymerization was carried out in a TDB-120 (SIA BIOSAN, Riga, Latvia) dry block thermostat at gradually increasing temperatures: +37 °C for 24–72 h, +45 °C for 24 h, +60 °C for 24 h. Ultrathin 70 nm sections were obtained with a Leica EM UC7 Ultracut (Leica Microsystems GmbH (Germany)). Sections were placed on Formvar[®]-coated grids and stained with aqueous 1% uranyl acetate for 6 min, followed by 1% lead citrate for 3 min prior to imaging with JEM-1400 (JEOL Ltd., Tokyo, Japan) or JEM-2100 (JEOL Ltd., Tokyo, Japan) transmission electron microscopes at the Core Facility Center for Molecular and Cell Technologies of St. Petersburg State University, Russia.

2.7. Atomic Force Microscopy (AFM)

Approximately 2–5 ciliate cells, pre-starved for 24 h in sterile lettuce broth, were collected with a glass capillary in a small drop of medium and placed on a slide. The cells were then disrupted with a sterile 26 G needle under a stereomicroscope control, air-dried and then examined in a semi-contact mode with Atomic Force Microscope NTEGRA Aura (NT MDT, Russia) at the Core Facility Center for Microscopy and Microanalysis of St. Petersburg State University, Russia.

2.8. Killer-Trait Assessment and Experimental Infection

In order to assess killer-trait, possibly provided to *Paramecium* strains by their bacterial endosymbionts, 10 symbiont-containing cells of the TRF-1 strain were placed together with 10 pre-washed cells of four endosymbiont-free *Paramecium* strains (Table 1) in 1 mL of sterile lettuce medium. The negative control was performed with 10 cells of each test *Paramecium* strain placed separately under similar conditions. The number of live cells was counted in 1 h and 24 h with a stereomicroscope.

Experimental infection was carried out as follows. The suspension of crushed symbiont-containing ciliate cells was made by multiple passes of 2.5 mL of the abundant TRF-1 culture through a 26 G needle syringe. The absence of viable ciliate cells was checked under a stereomicroscope. Then, 500 µL of the endosymbiont-containing suspension was added to 50 pre-starved cells of each recipient strain in 100 µL of sterile lettuce medium.

The presence/absence of endosymbionts in the cytoplasm of the test *Paramecium* cells was checked following 1 h and 24 h with DIC.

2.9. Data Availability

DNA sequences obtained in this study were deposited at Genbank/ENA/DDBJ [46] under accession numbers: OR144032, OR144033, OR144034, OR229901, OR229902, OR239107, OR239108, OR239109, OR243302, OR243303, OR243304.

3. Results

3.1. Host Identification

The main morphological characteristics of the ciliate host cells observed with DIC (cell shape, way of movement, position of the buccal cavity) corresponded to the *Paramecium* morphotype according to Fokin [32]. The molecular verification of each studied ciliate strain species was carried out using 2 genetic markers—18S rRNA and COI gene sequences [6,21–23]. The standard nucleotide BLAST search [47] of the newly obtained sequences (1223–1748 nt long for 18S rRNA genes) demonstrated that the host ciliate strain VL18-4 (accession numbers OR144033, OR239109) belonged to the *P. caudatum* species, the highest similarity score with *P. caudatum* sequences AF217655.1 [60], AB252003.1 [61] being 99.89%, while strains BMS16-3 and TRF-1 (accession numbers OR144034, OR144032, OR239108, OR239107) belonged to the *P. nephridiatum* species, the sequences being 100% identical to the *P. nephridiatum* sequences MK764889.1 [15] and OQ548095.1 [62]. As for the obtained sequences for COI genes (648–734 nt long), the sequence OR243302 showed 100% identity with *P. caudatum* sequences NC_014262.1 [63] and FJ905148.1 [36], while the closest BLAST search results for OR243303 and OR243304 were FJ905151.1 [36] and MG589326.1 [21], with similarity scores of 100% and 99.42%, respectively. Phylogenetic positions of the studied ciliate strains were confirmed by constructing corresponding ML trees (see Supplementary Materials Figures S1 and S2).

3.2. Living Host Cells Observations

Observations made with DIC and phase contrast microscopy revealed that the strains VL18-4, BMS16-3 and TRF-1 harbored morphologically similar non-motile spindle-shaped flagellated cytoplasmic bacteria with peculiar refractive granules (Figure 1A–D,F–I). Strain VL18-4 hosted only this type of endosymbionts, while the cytoplasm of cells of the BMS16-3 and TRF-1 strains was additionally inhabited by small motile rod-shaped bacteria (Figure 1B,E).

The symbiotic association of strain VL18-4 was maintained for more than 4 years and finalized in spontaneous loss of endosymbionts with subsequent flourishing of the symbiont-free ciliate culture for more than 6 years (to date).

The association of *P. nephridiatum* with two different cytoplasmic endosymbionts, spindle-shaped rods and straight rods was ultimately stable and has been successfully maintained by the strain TRF-1 for more than 5 years under laboratory conditions (to date) and by the strain BMS16-3 for more than 2 years, the latter becoming extinct by the end of this period.

3.3. Spindle-Like Endosymbiont with a Refractive Granule Inhabiting the Cytoplasm of *Paramecium caudatum* and *Paramecium nephridiatum* Strains

3.3.1. Morphology and Biology

Endosymbionts were abundantly and evenly distributed throughout the *Paramecium* cytoplasm with no observed preference to any ciliate cell compartment (Figure 1A). Average bacterial cell size varied depending on the host strain species: *P. caudatum* strain VL18-4 harbored bacteria 1.1–1.8 (av. 1.4) × 3.2–6.6 (av. 4.8) µm in size, *P. nephridiatum* strain BMS16-3 harbored bacteria 1.2–1.9 (av. 1.5) × 2.6–4.5 (av. 3.6) µm in size and *P. nephridiatum* strain TRF-1 strain harbored bacterial cells 1.1–1.7 (av. 1.4) × 2.5–5.0 (av. 3.7) in size. Thus, notably longer forms of the endosymbionts (with relatively the same width) inhabited

the cytoplasm of the *P. caudatum* strain (VL18-4) (Figure 1A,H), than those inhabiting the cytoplasm of the *P. nephridiatum* strains (BMS16-3 and TRF-1) (Figure 1B–D,F,G). An increase of the cultivation temperature from +16 °C to +23 °C led to the conversion of cytoplasmic symbionts of the *P. caudatum* strain VL18-4 to filamentous forms up to 55–60 µm in length, still non-motile (Figure 1I).

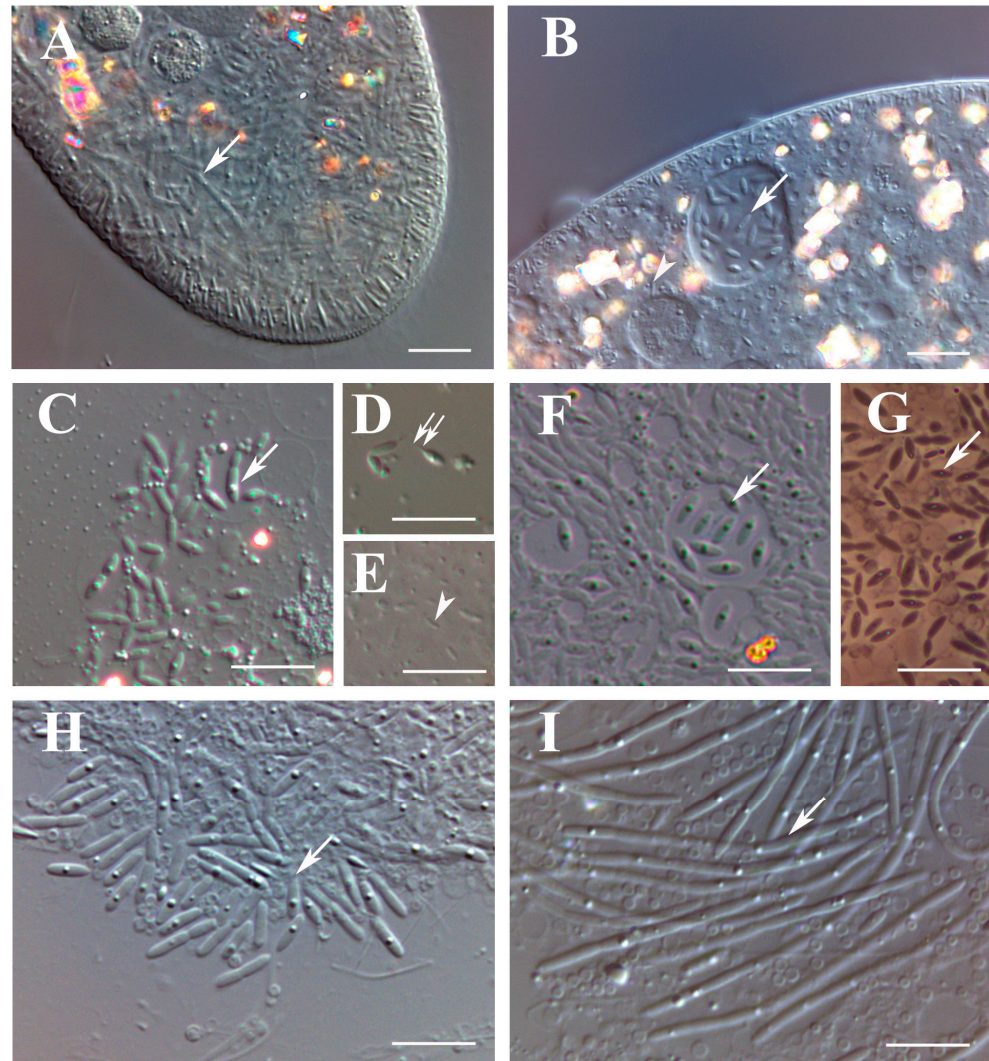


Figure 1. Bacterial endosymbionts in *P. caudatum* strain VL18-4 and *P. nephridiatum* strains BMS16-3 and TRF-1, living cell observations. All images, except (G), were made with DIC, (G)—phase contrast. (A)—Living cell of *P. caudatum* strain VL18-4. (B)—Living cell of *P. nephridiatum* strain BMS16-3, the spindle-shaped bacteria are seen enclosed in a vacuole. (C–E)—Bacteria released from the crushed *P. nephridiatum* cell, strain TRF-1. (C)—Spindle-shaped bacteria. (D)—A spindle-shaped bacterium with a “tail” formed by numerous flagella. (E)—Small rod-like bacteria. (F,G)—Spindle-shaped bacteria released from the crushed *P. nephridiatum* cell, strain BMS16-3. (H,I)—Endosymbionts released from the crushed *P. caudatum* cell, strain VL18-4. (H)—Cells cultivated at normal temperature. (I)—Cells cultivated at elevated temperature. Spindle-shaped bacteria with a refractive granule are shown with an arrow, double arrow points to the bacterial “tail”. Small rod-shaped bacteria are marked with an arrowhead. Scale bar 10 µm.

Spindle-like symbiotic bacteria were obligatorily enclosed into membrane-bound vesicles, individually or, rarely, in groups (Figure 1B,F). These endosymbionts, despite being non-motile, demonstrated the presence of numerous flagella forming a monopolar bundle (Figure 1D).

A single spherical refractive granule, well-detectable with DIC, was located in the center of most bacterial cells. During binary fission, the simultaneous presence of two granules displaced to the distal poles of daughter cells could sometimes be observed. Multiple refractive granules were common only for filamentous forms of *P. caudatum* strain VL18-4 symbionts (Figure 1I).

3.3.2. Fine Structure

In TEM sections, symbionts showed a typical morphology of Gram-negative bacteria with a well-detectable double membrane cell wall (Figure 2A–F). The cytoplasm had moderate electron density with notable ribosomes, free electron-lucid areas and no nucleoid observed.

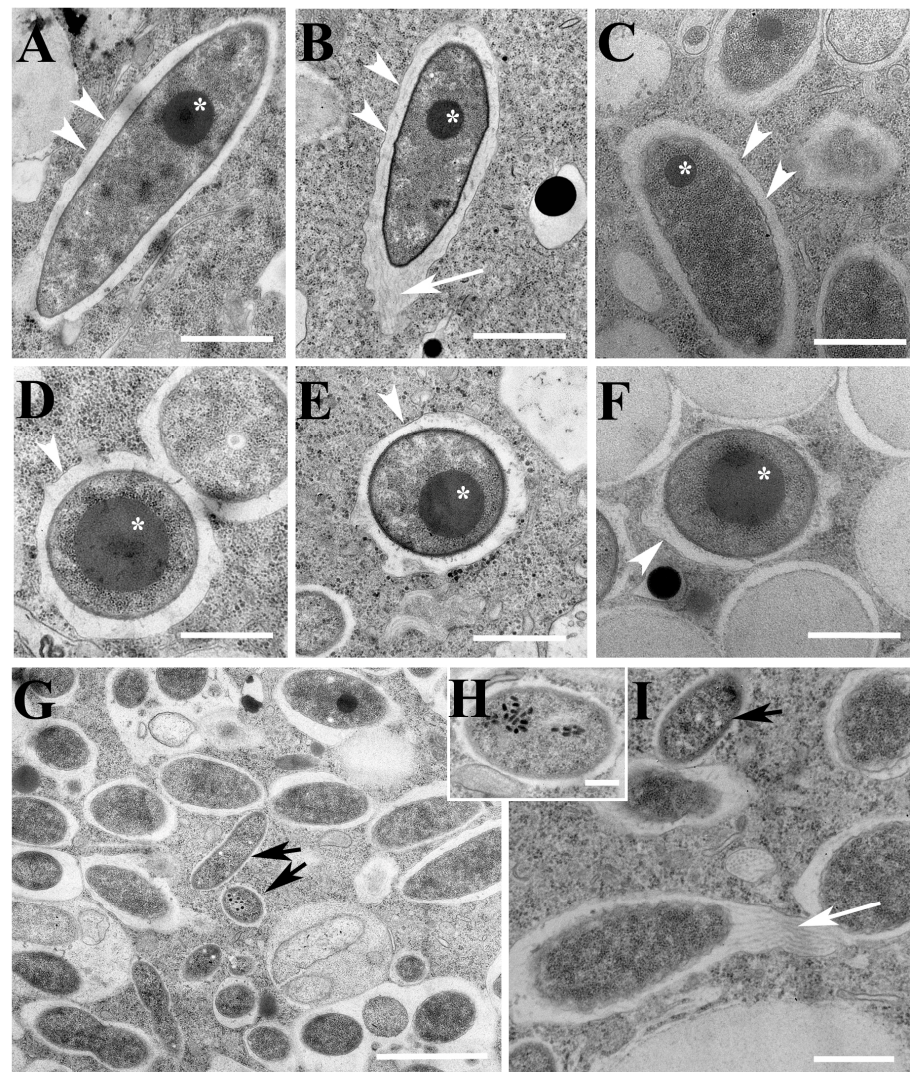


Figure 2. Endosymbionts in *P. nephridiatum* strains BMS16-3 and TRF-1 and *P. caudatum* VL18-4 strain, TEM. (A,D)—Spindle-shaped endosymbiont in the cytoplasm of *P. caudatum* VL18-4 strain. (B,E)—Spindle-shaped endosymbiont in the cytoplasm of *P. nephridiatum* strain BMS16-3. (C,F)—Spindle-shaped endosymbiont in the cytoplasm of *P. nephridiatum* strain TRF-1. (A–C)—Longitudinal section. (D–F)—Cross-section. (G,I)—Spindle-shaped and rod-shaped endosymbionts in the cytoplasm of *P. nephridiatum* strain TRF-1. (H)—Rod-shaped endosymbiont with viral particles in its cytoplasm. Arrowheads mark the membrane of the symbiontophorous vacuole. Arrows point to bacterial flagella. The inclusion body is marked with an asterisk. Scale bar 1 µm (A–C), 500 nm (D–F,I), 2 µm (G) and 200 nm (H).

The study of TEM sections confirmed the intra-vesicle location of the spindle-like symbiotic bacteria (Figure 2A–F). The space between the bacterial cell wall and the membrane of the symbiontophorous vacuole was filled with numerous flagella emerging all along the bacterial cell that joined together and twisted, finally forming a bundle at one of the bacterial poles (Figure 2B). A helical bundle $\sim 3.0 \mu\text{m}$ long was also clearly visualized with AFM (Figure 3B,C). Thus, the pattern of the symbionts' flagellar arrangement could be defined as peritrichous.

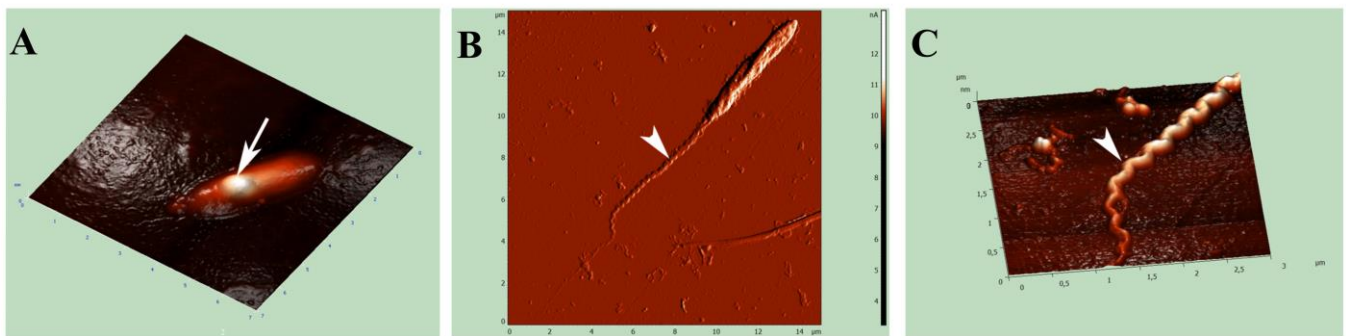


Figure 3. Spindle-shaped bacteria, AFM. (A)—A bacterium released from a cell of *P. nephridiatum* strain BMS16-3, 3D reconstruction. A conspicuous inclusion body is shown with an arrow. (B)—A bacterium released from a cell of *P. caudatum* strain VL18-4; a bundle of twisted flagella is marked with an arrowhead. (C)—The bundle of flagella, 3D reconstruction. Scale in μm .

Inclusions, previously detected with DIC as large refractive granules, were present in most examined bacterial TEM sections originating from all three ciliate strains. They appeared as evenly electron-dense bodies up to 500 nm in diameter with a regular circle shape and clear borderlines. These inclusions were freely located in the bacterial cytoplasm, having no visible boundary membranes (Figure 2A–F). Their edges could be visualized in rare TEM sections, sometimes giving the inclusion a polygonal shape (Figure 2F).

3.3.3. Chemical Nature of the Inclusion Bodies

Cytochemical staining was performed in an attempt to elucidate the nature of symbiotic inclusion bodies. Amido Black 10B staining resulted in bright blue coloring of the granules (Figure 4A,B), while bacterial cytoplasm remained transparent, suggesting the protein nature of the studied inclusion bodies. The inclusion bodies were also positive with eosin staining, supporting the data obtained with Amido Black (Figure 4C). Sudan Black B and Congo Red staining gave negative results (not shown), thus excluding the polyhydroxybutyrate (PHB) or amyloid nature of granules, respectively.

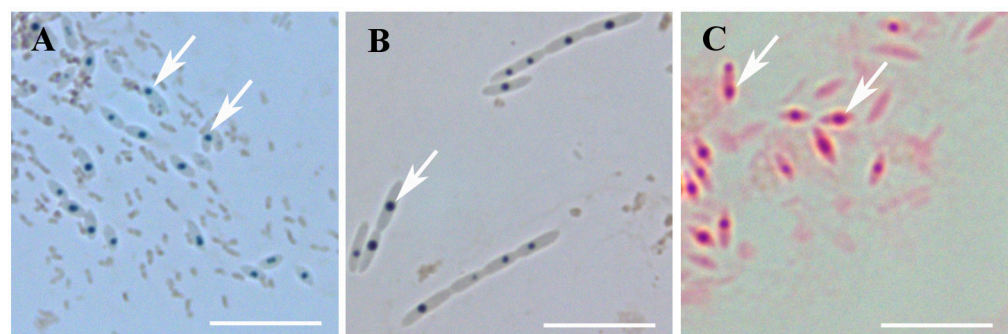


Figure 4. Histochemical staining of the spindle-shaped endosymbiotic bacteria, bright field microscopy. (A,C)—*P. nephridiatum* strain BMS16-3. (B)—*P. caudatum* strain VL18-4. (A,B)—Amido Black staining. (C)—Eosin staining. Arrows point to the inclusion bodies revealed with both techniques. Scale bar 10 μm .

3.3.4. Molecular Identification and Phylogeny

For total DNA samples, extracted from *Paramecium* strains VL18-4, BMS16-3 and TRF-1, amplification of the endosymbiotic 16S rRNA gene fragments was carried out. Subsequent cloning of PCR products and analysis of the obtained data resulted in a selection of the sequences, 1474–1536 bp long depending on a strain, with a cross-identity score between samples min. 99.7% (accession numbers OR243302, OR243303, OR243304). Such close similarity of the obtained sequences provides evidence for the presence of one and the same bacterial endosymbiont in three *Paramecium* strains belonging to two different species—*P. caudatum* and *P. nephridiatum*.

Based on the selected sequences, the species-specific oligonucleotide probe Pslyt1088 was designed for FISH experiments and tested at 0%, 15% and 30% formamide concentrations. FISH confirmed the presence of spindle-like rod-shaped bacteria evenly and abundantly distributed in the cytoplasm of all inspected ciliate strains cells (Figures 5 and 6).

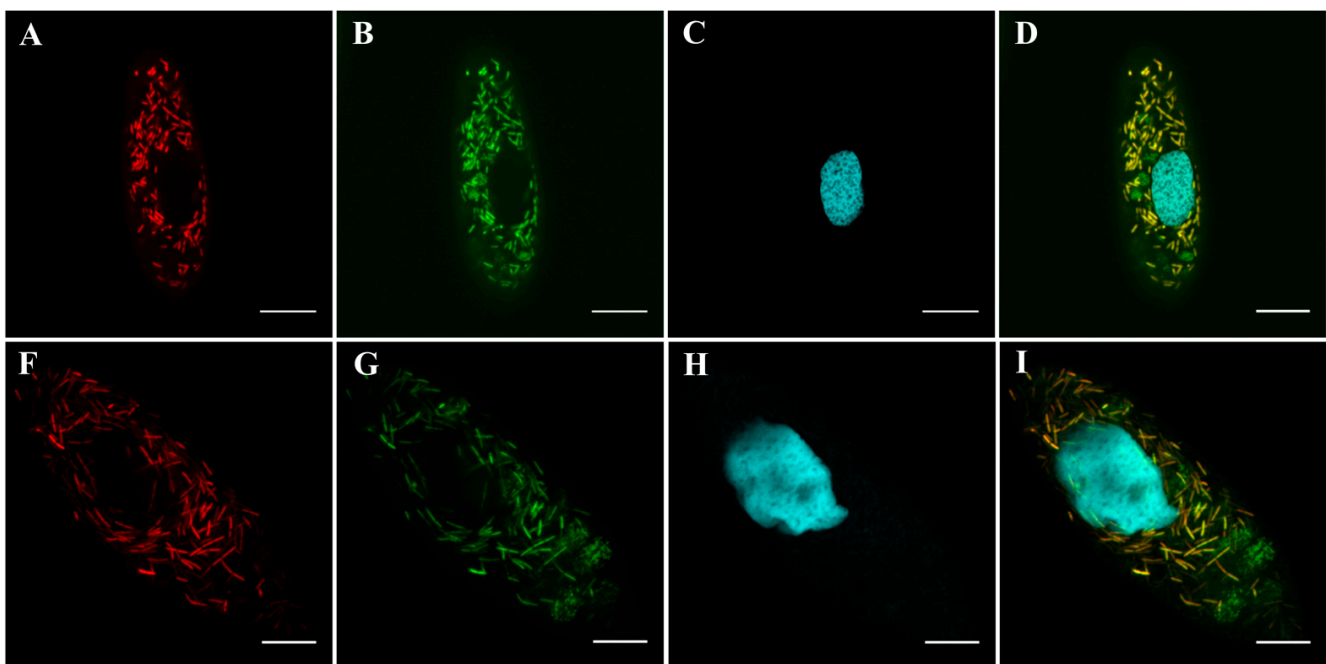


Figure 5. Fluorescence *in situ* hybridization of the endosymbionts in the paramecium cells, CLSM. *P. nephridiatum* strain BMS16-3 (upper row), *P. caudatum* strain VL18-4 (lower row). (A,F)—Cells labelled with Pslyt1088 probe, red signal. (B,G)—Universal eubacterial probe Eub338, green signal. (C,H)—DAPI, cyan. (D,I)—merged image. Scale bar 20 μ m.

The highest identity score (91.73%) of the newly obtained endosymbiotic 16S rRNA gene sequences with standard BLAST search was matched with “*Ca. Euplotella sexta*” (LR585343.1), member of the family “*Candidatus* Midichloriaceae” (order Rickettsiales, class Alphaproteobacteria). Subsequent phylogenetic analysis within the family “*Ca. Midichloriaceae*” (29 representatives), with 17 other Rickettsiales as an outgroup, resulted in the construction of an ML (TVMe+I+G4 automatically chosen best-fit substitution model) tree, where studied sequences were located within an AF clade of “*Ca. Midichloriaceae*” family (Figure 7). This clade consists exclusively of cytoplasmic endosymbionts of Ciliophora [23]. The studied sequences formed a sister clade to “*Ca. Euplotella sexta*”, a cytoplasmic endosymbiont of *Euplotes octocarinatus* [64].

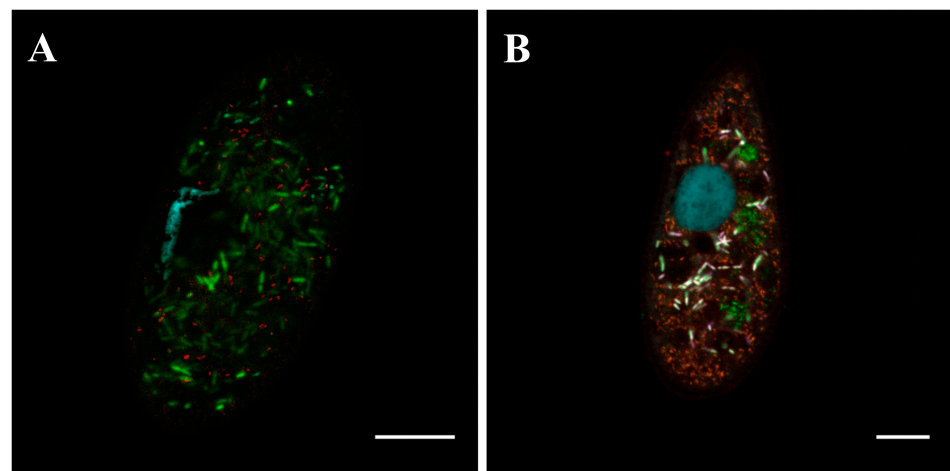


Figure 6. Fluorescence *in situ* hybridization of the endosymbionts in the paramecium cells, CLSM. Only merged images are shown. (A)—*P. nephridiatum* strain BMS16-3 labeled with Pslyt1088 probe (FAM, green signal) and MegVen1226 (Cy3, red signal) and counterstained with DAPI (cyan). (B)—*P. nephridiatum* strain TRF-1 labeled with Pslyt1088 probe conjugated to Cy5, MegVen1226 (Cy3), Eub338 (FAM) and counterstained with DAPI (cyan). *Ps. multiflagellatum* appears white, *Ca. Megaira venefica*—orange, food bacteria in the food vacuoles—green. Scale bar 20 μm.

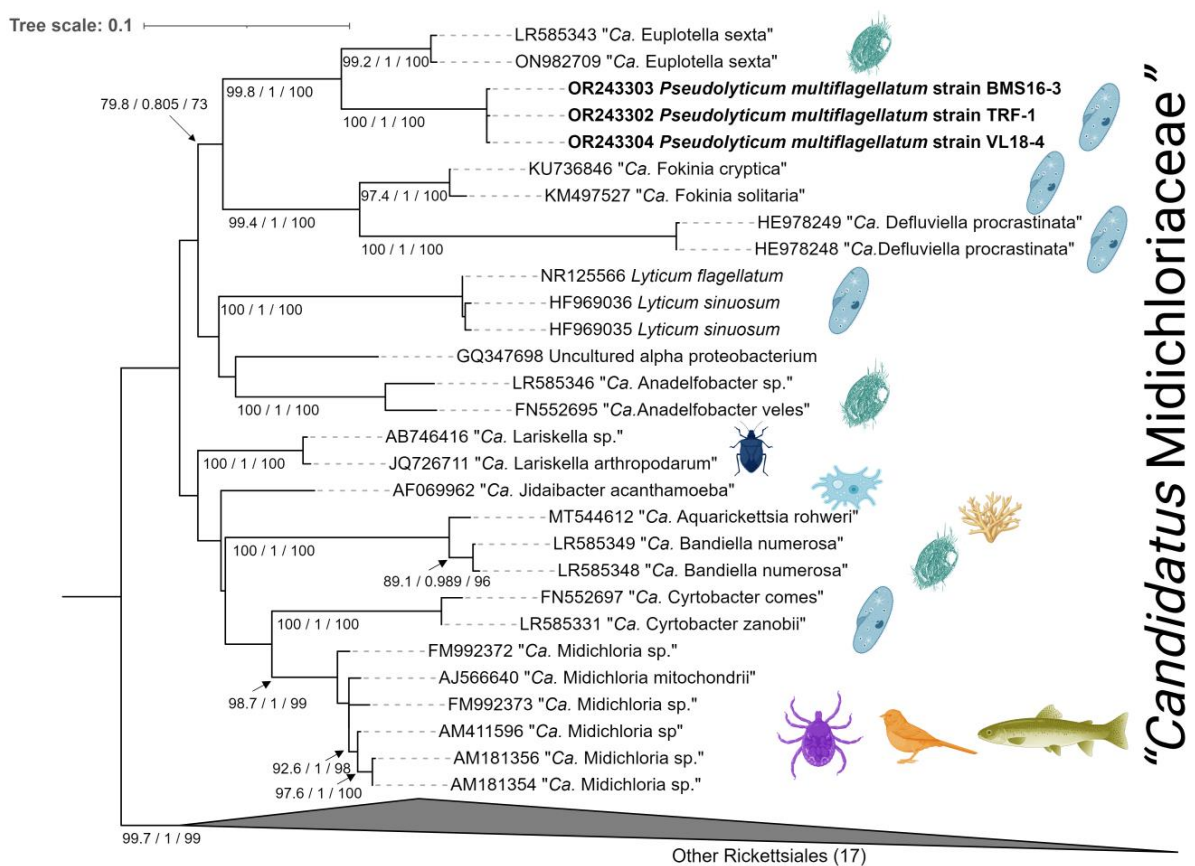


Figure 7. Maximum likelihood (ML) phylogenetic tree with the TVMe+I+G4 substitution model based on 16S rRNA sequences. Numbers associated with the nodes represent values of SH-like aLRT/aBayes parametric test/ML bootstrap (only values above 70/0.7/70 are shown, respectively). Reported in bold are sequences characterized in the present study. Numbers in brackets indicate the number of sequences representing clade. Identified hosts are shown as silhouettes. Created with BioRender.com (accessed on 30 May 2023).

3.3.5. Killer-Trait Assessment

The killer-trait assay of the TRF-1 strain's endosymbionts did not show any decrease in the test ciliate cell number indicating the absence of killer effect. Endosymbionts did not demonstrate any infectious capacity either.

3.4. Rod-Shaped Small Motile Endosymbionts Inhabiting the Cytoplasm of *Paramecium nephridiatum* Strains

3.4.1. Biology and Morphology

Besides the non-motile spindle-like endosymbionts, the cytoplasm of *P. nephridiatum* BMS16-3 and TRF-1 cells harbored numerous small (0.4–0.5 μm wide and 1.1–2.5 μm long) straight rod-shaped motile bacteria. These endosymbionts showed no preference for any cellular compartment and were never enclosed in membrane bound vesicles. The cells demonstrated non-directional tumbling movement easily detectable with DIC in the crushed pre-immobilized ciliates.

3.4.2. Fine Structure

The following typical morphological features of rod-shaped bacteria were observed in TEM sections obtained from *P. nephridiatum* BMS16-3 and TRF-1 strains: double cell-wall with wavy unclear outlines, homogenous cytoplasm of moderate electron density with notable ribosomes. No nucleoid or inclusion bodies were detected. Endosymbionts lay “naked” in the *P. nephridiatum* cytosol, were always surrounded by a thin electron-lucid area devoid of host ribosomes and had no detectable flagella (Figure 2G,I).

Along with the representatives that had typical morphology, some of the small rod-shaped bacteria in the cytoplasm of the *P. nephridiatum* TRF-1 strain showed strikingly different features: had more rounded shapes, smoother outer contours of the double-cell wall and clearer electron-lucid area surrounding bacteria. Most of such “atypical” endosymbionts contained numerous grouped electron-dense particles ~60 nm in diameter resembling phages, while flagella or a capsules were still not detected (Figure 2G,H). The obtained TEM images did not allow us to exclude the possible presence of the third species of the endosymbiotic bacteria in the cytoplasm of *P. nephridiatum* TRF-1 strain.

3.4.3. Molecular Identification and Phylogeny

The second set of 16S rRNA gene fragments from the DNA samples of the *P. nephridiatum* BMS16-3 and TRF-1 strains was amplified and subsequently cloned. Obtained sequences, min. 1479 bp long each, turned out to be more than 99% similar.

A standard BLAST search showed 99.1–99.66% identity of the newly obtained sequences (accession numbers: OR229901, OR229902) with “*Ca. Megaira venefica*” entries (MK775139.1, MK775140.1, LR585347.1). Subsequent phylogenetic analysis revealed clustering of newly obtained 16S rRNA gene sequences into clade C, “*Ca. Megaira venefica*” (MK775139.1, MK775140.1, LR585347.1) of the genus “*Ca. Megaira*” (family *Rickettsiaceae*, order *Rickettsiales*, class *Alphaproteobacteria*) [21] (see Supplementary Materials, Figure S3). FISH with species-specific oligonucleotide probe 16S_MegVen1226 [15] confirmed the presence of numerous small rod-shaped cytoplasmic bacteria in every tested cell of *P. nephridiatum* BMS16-3 and TRF-1 strains (Figure 6).

Analysis of more than 30 PCR product clones from total DNA samples of the TRF-1 strains in an attempt to identify the putative third endosymbiont (with “atypical” morphology in TEM sections) did not reveal any additional 16S rRNA gene sequences.

4. Discussion

4.1. Phylogeny and Taxonomy of the Spindle-like Endosymbiont

Non-motile peritrichous spindle-like endosymbionts residing in the cytoplasm of the *P. caudatum* VL18-4 strain and *P. nephridiatum* BMS16-3 and TRF-1 strains contained peculiar inclusion bodies, clearly detectable with DIC as refractive granules, and were obligatorily enclosed in membrane-bound vesicles, individually or in groups. Longer forms of the

bacteria inhabited the cytoplasm of the *P. caudatum* strain VL18-4 (average length ~4.8 μm), and shorter forms inhabited the cytoplasm of *P. nephridiatum* strains BMS16-3 and TRF-1 (average length ~3.6 μm) with relatively the same width (av. ~1.4 μm). In addition to the difference in size, endosymbionts solely of the *P. caudatum* VL18-4 strain were able to transform into filamentous forms up to 55–60 μm in length in response to an increase in cultivation temperature. Thus, the appearance of these endosymbionts (excluding the observed existence of filamentous forms) almost perfectly corresponded to the descriptions provided earlier for *Pseudolyticum multiflagellatum* by Boss et al. [25] and for *Pseudolyticum minutus* by Fokin [27].

The detection of similar endosymbiotic 16S rRNA gene sequences in three studied symbiont-containing *Paramecium* strains (cross-identity min. 99.7%) suggested the presence of the same bacterial species in their cytoplasm, despite the morphological heterogeneity demonstrated by endosymbionts. This assumption was confirmed by FISH experiments with the newly designed species-specific oligonucleotide probe Lyt1088. Phylogenetic analysis revealed the spindle-like symbiont to be affiliated with the family “*Ca. Midichloriaceae*” of the order Rickettsiales, where it forms a well-supported monophyletic group within the AF-clade [23] together with other genera of ciliate endosymbionts: “*Ca. Euplotella sexta*” from the cytoplasm of *Euplotes octocarinatus* [64], “*Ca. Fokinia*” from the cytoplasm of *P. biaurelia* [65] and “*Ca. Defluviella procrastinata*” inhabiting the cytoplasm of *P. nephridiatum* [66]. The 16S rRNA gene sequences of the three isolates (VL18-4, BMS16-3 and TRF-1) demonstrated the highest identity score (91.73%) with “*Ca. Euplotella sexta*” (LR585343.1), which makes it possible to allocate the spindle-like endosymbiont to a separate genus with a single species according to commonly used molecular thresholds [67].

Molecular verification allowed us to identify non-motile peritrichous spindle-like endosymbionts from the cytoplasm of the *P. caudatum* strain VL18-4 and *P. nephridiatum* strains BMS16-3 and TRF-1 as a single species, despite their host-dependent phenotypic variations in size, conditional morphotypic plasticity (e.g., capability of filamentation) and the capacity to colonize distinct *Paramecium* species. Thus, it seems reasonable to merge the descriptions of *Pseudolyticum multiflagellatum*, a bacterial endosymbiont from the cytoplasm of *P. caudatum* provided by Boss et al. in 1987 [25], *Pseudolyticum minutus*, a bacterial endosymbiont from the cytoplasm of *P. nephridiatum* provided by Fokin in 1988 [27] and cytoplasmic endosymbiont inhabiting *P. caudatum* strain VL18-4 and *P. nephridiatum* strains BMS16-3 and TRF-1 provided in this study into a unified description of the single species—*Pseudolyticum multiflagellatum*.

4.2. Polymorphism of *Pseudolyticum multiflagellatum*

Conditional filamentation is an adaptive trait of many bacteria, including representatives of phyla Proteobacteria, when long, thread-like cells lacking peptidoglycan septa appear in a culture as a result of bacterial lateral growth under suppressed cell division [68]. This mechanism is often used by bacteria as a survival strategy in toxic or stressful environments and can be induced by different factors, e.g., cold temperature or heat shock, high osmolarity, antibiotic exposure, extreme pH, UV exposure, etc. [69]. Filamentation is also used by multiple bacteria as a strategy to escape predation by protists [68,70] or it even can be used for the cell-to-cell spread of intracellular bacterial pathogens [71]. Drug-induced filamentation has been observed in an intranuclear endosymbiont of *Paramecium multimicronucleatum*—“*Ca. Trichorickettsia mobilis*” [22]. This representative of the order Rickettsiales is commonly characterized as constantly moving short rods, but exposure to ampicillin (irreversible inhibitor of bacterial transpeptidase blocking bacterial cell wall formation), even at the lowest doses, induced transformation of these bacteria into non-motile filamentous forms. Filamentation has not been previously described in the bacteria of the family “*Ca. Midichloriaceae*”, represented exclusively by endosymbiotic species.

In our study, rising the cultivation temperature from +16 °C to +23 °C triggered filamentation of *Ps. multiflagellatum* inhabiting exclusively cells of the *P. caudatum* VL18-4 strain later resulting in a complete loss of endosymbionts. The observed transformation

of *Ps. multiflagellatum* to filamentous form could have emerged as a certain reaction to heat shock with the subsequent extinction of bacterial culture due to disadaptation to unfavorable environmental conditions. Interestingly, endosymbionts of *P. nephridiatum* BMS16-3 and TRF-1 strains did not perform a similar response to the same temperature shift, which demonstrates another host-specific phenotypic trait.

4.3. The Presence of Flagella in *Pseudolyticum multiflagellatum*

Pseudolyticum multiflagellatum is a rare flagellated representative of the family “*Ca. Midichloriaceae*”. While flagellar genes have been reported in most “*Ca. Midichloriaceae*” [23], only *Lyticum* has been previously described as a possessor of visible corresponding structures—numerous flagella [72]. Like *Lyticum*, both observed morphotypes of *Pseudolyticum multiflagellatum*, spindle-like rods and filamentous forms, were peritrichous, resided in symbiontophorous vacuoles in the host cytoplasm and did not show any ability to move either inside the vacuoles or outside the ciliate cell. Further study of the role of flagella in initiating host–symbiont relationships is required.

4.4. The Nature of the Inclusion Bodies and Its Functions

Peculiar inclusions in the cytoplasm of *Pseudolyticum multiflagellatum* cells, detected with DIC as highly refractive granules, in TEM sections showed a high electron density and structure somewhat similar to protein inclusions found in bacteria (for review, see [73,74]). Their matrix can be characterized as homogenous, though with no crystalline lattice observed clearly. Despite the absence of any detectable boundary membranes, the inclusions usually maintained a well-defined circular shape with distinct borders. Exactly the same images of bacterial inclusions were obtained earlier in TEM sections of *Ps. multiflagellatum* and *Ps. minutus*, examined by Boss et al. [25] and Fokin [27], respectively. A polygonal shape of inclusions could be suspected in several ultrathin sections in our study (Figure 2F).

Amido Black 10B and eosin staining carried out in our work confirmed the protein nature of the inclusion bodies (Figure 3) [57], which contradicted the findings of Boss and al., who concluded that the inclusions were lipid based on their positive staining with Sudan black B [25]. Our attempt to perform lipophilic staining with Sudan black B failed. In TEM sections, lipophilic inclusions usually appear as electron-transparent structures of different shapes and sizes without any visible internal content but with a single boundary layer (for review, see [75,76]), which is strikingly different from the TEM images of *Ps. multiflagellatum* inclusions obtained in our study or earlier [25,27]. Thus, the positive reaction of the inclusion bodies with Sudan black B staining [25] could be explained by methodological shortcomings causing the non-specific binding of a lipophilic dye to protein inclusions.

The results of cytochemical staining and ultrastructural analysis suggested that the inclusion bodies may consist of an amorphous mass of non-functional misfolded proteins. However, Congo Red staining showed no amyloid-like properties of the inclusion bodies. The function of these bodies still remains unclear, allowing only suggestions to be made.

The refractive properties of the inclusion bodies are similar to R-bodies, first discovered in the cytoplasm of endosymbiotic bacteria of *Paramecium*. R-bodies are protein inclusions with sheaths made of highly insoluble protein hypercoiled ribbons [77]. Properly folded, they usually appear in TEM sections as multilayered tightly rolled hollow cylindrical structures. The presence of functional endosymbiotic R-bodies is a prerequisite for the manifestation of a killer trait in *Paramecium* host strains [78,79]. Initially discovered in *Caedibacter*, R-bodies were later found in a number of other symbiotic and non-symbiotic members of Proteobacteria, performing functions that are not always obvious [80–82]. Homologs of Reb genes encoding protein components of R-bodies are widespread in members of Proteobacteria, but have not been yet described among representatives of the order Rickettsiales [83], which makes them unlikely to exist in *Ps. multiflagellatum*. Moreover, the lack of killer-traits in *Paramecium* cells bearing *Ps. multiflagellatum*, as shown

by our experiments and by the previous studies [25,27], and the absence of the typical coiled ribbon in TEM images, makes this suggestion doubtful.

Probably, the inclusion bodies could consist of fully functional proteins, perhaps regularly assembled. Regularity of the protein structure could perfectly explain detected peculiarities of their ultrastructure—constantly clear boundaries of the inclusions and their polygonal shape in some TEM sections (Figure 2F).

The crystalline protein state is exploited by a number of entomopathogenic Gram-positive spore-forming bacteria for long-term storage of their toxins while the endospores remain in the environment [84–87]. In the gut of an insect, the toxins are released and kill the host. However, similar crystalline inclusions found in entomopathogenic Gram-negative bacteria, e.g., *Photorhabdus luminescens* and *Xenorhabdus nematophilus*, appeared to miss direct insecticidal activity, so their role as providers of essential amino-acids or developmental signals for mutualistic nematodes was suggested [88,89]. Considering that *Ps. multiflagellatum* does not seem to harm perceptibly its host ciliate, direct toxic anti-ciliate action of inclusion bodies proteins is doubtful. The inclusion bodies might possibly serve for the storage of some proteins for the survival of the endosymbiont in case it is released from the host. Although the way of the host infection with *Ps. multiflagellatum* is unknown as yet, its presence in different host species suggests the possibility of horizontal transfer.

Anyway, further studies are required to unravel the functions of the proteins constituting the inclusion bodies in *Ps. multiflagellatum*.

4.5. Polymorphism in “*Ca. Megaira venefica*”

The second endosymbiont inhabiting the cytoplasm of the *P. nephridiatum* strain TRF-1, “*Ca. Megaira venefica*”, in TEM sections demonstrated the presence of two morphological variants. “Typical” representatives, similar to the bacteria found in the cytoplasm of *P. nephridiatum* strain BMS16-3, differed in size and shape from the “atypical” forms, often containing viral particles and found solely in the cytoplasm of the TRF-1 strain. Although the aspect of the “atypical” forms at first connoted the presence of the third species of endosymbiotic bacteria in this strain, an analysis of more than 30 clones of amplified 16S rRNA gene fragments obtained from total DNA samples isolated twice from *P. nephridiatum* strain TRF-1 proved this assumption wrong, since no additional 16S rRNA gene fragments other than those belonging to *Ps. multiflagellatum* and “*Ca. Megaira venefica*” were detected. Thus, “*Ca. Megaira venefica*” can strikingly transform its morphology due to some factors, e.g., viral invasion. Our observations are consistent with those made earlier for some virus-containing cytoplasmic endosymbionts of *Paramecium nephridiatum* [90], *Paramecium calkinsi* [91], *Ophryoglena* sp. [92], *Blepharisma japonicum* [93] and for symbiotic macronuclear alfa-proteobacteria of *Frontonia leucas* [94]. Unfortunately, those articles did not contain molecular data to identify the discovered bacterial symbionts.

Interestingly, viral infection has been recently demonstrated in a closely related species, *Megaira polyxenophila* harbored by the flagellate *Cryptomonas gyropirenoidea* [95]. The *Megaira*-infecting phage, MANkyphage, belongs to the clade that is widely distributed in various environments, freshwater, brackish and marine [95]. The phage infecting *Ca. Megaira venefica* is likely to belong to the same clade.

5. Conclusions

In this study, based on the analysis of the 16S rRNA gene, we proved that spindle-shaped endosymbiotic bacteria with an inclusion body harbored by *P. caudatum* and *P. nephridiatum* belong to one and the same species, *Pseudolyticum multiflagellatum*, originally described on the basis of morphological features only [25]. The phylogenetic analysis showed that this species was affiliated to the family “*Ca. Midichloriaceae*” (Rickettsiales). This is another flagellated representative of this family.

Differences in the appearance (in size and shape) of the same endosymbiont species inhabiting different hosts might be a result of its adaptation to the life within a particular

host, the bigger size of the host cell possibly allowing for the appearance of longer bacterial forms, especially under temperature shifts.

Viral infection of the other endosymbiont, “*Ca. Megaira venefica*”, leads to the changes in bacterial morphology. Thus, both endosymbiotic bacteria, *Ps. multiflagellatum* and “*Ca. Megaira venefica*”, demonstrate polymorphism, albeit due to different causes.

One of the strains analyzed in this study is a good example of a complex symbiotic system, combining two partners occupying the same host compartment (the cytosol), and at the same time partly resembling a nested toy, one of the partners bearing occasional phage particles. The complex symbiotic systems of this kind are a challenging object of research due to apparently complicated cross-talk between the partners ensuring the stability of the whole system.

Supplementary Materials: The following supporting information can be downloaded at: <https://www.mdpi.com/article/10.3390/d15080924/s1>, Figure S1: Maximum likelihood (ML) phylogenetic tree with the GTR+F+I+G4 substitution model based on 18S rRNA sequences; Figure S2: Maximum likelihood (ML) phylogenetic tree with the GTR+F+I+G4 substitution model based on mitochondrial COI gene sequences; Figure S3: Maximum likelihood (ML) phylogenetic tree with the TPM3u+F+I+G4 substitution model based on 16S rRNA sequences.

Author Contributions: Conceptualization, E.S.; investigation, E.K. and A.K.; resources, N.L.; writing—original draft preparation, E.K.; writing—review and editing, E.K., A.K., E.S. and N.L.; visualization, A.K., E.K., E.S. and K.B.; supervision, E.S.; funding acquisition, E.S. All authors have read and agreed to the published version of the manuscript.

Funding: This research was funded by RSF grant number 22-24-00335 to E.S.

Institutional Review Board Statement: Not applicable.

Data Availability Statement: DNA sequences obtained in this study were deposited at Genbank/ENA/DDBJ.

Acknowledgments: One of the strains used in this study was collected at the Educational and Research station “Belomorskaya” (SPbU), White Sea, which would have been impossible without the kind support of its staff. The study was performed using the culture collection RC CCM of the Core Facility Center for Cultivation of Microorganisms. We are grateful to the specialists of the Core Facility Centers of SPbU “Microscopy and Microanalysis” and “Molecular and Cell Technologies” for their help in using the equipment, and especially to Anna Romanovich for sequencing. We would also like to thank Alexander Kudryavtsev for permission to use the facilities of “Laboratory of Cellular and Molecular Protistology” of Zoological Institute of Russian Academy of Sciences for cloning experiments.

Conflicts of Interest: The authors declare no conflict of interest. The funders had no role in the design of the study; in the collection, analyses, or interpretation of data; in the writing of the manuscript; or in the decision to publish the results.

References

1. Husnik, F.; Tashyreva, D.; Boscaro, V.; George, E.E.; Lukeš, J.; Keeling, P.J. Bacterial and Archaeal Symbioses with Protists. *Curr. Biol.* **2021**, *31*, R862–R877. [[CrossRef](#)] [[PubMed](#)]
2. Dziallas, C.; Allgaier, M.; Monaghan, M.G. Act Together—Implications of Symbioses in Aquatic Ciliates. *Front. Microbiol.* **2012**, *3*, 288. [[CrossRef](#)] [[PubMed](#)]
3. Fokin, S. Bacterial Endocytobionts of Ciliophora and Their Interactions with the Host Cell. *Int. Rev. Cytol.* **2004**, *236*, 181–249.
4. Görtz, H.-D. Symbiotic Associations Between Ciliates and Prokaryotes. In *The Prokaryotes: Volume 1: Symbiotic Associations, Biotechnology, Applied Microbiology*; Dworkin, M., Falkow, S., Rosenberg, E., Schleifer, K.-H., Stackebrandt, E., Eds.; Springer: New York, NY, USA, 2006; pp. 364–402. ISBN 978-0-387-30741-1.
5. Fokin, S. Frequency and Biodiversity of Symbionts in Representatives of the Main Classes of Ciliophora. *Eur. J. Protistol.* **2012**, *48*, 138–148. [[CrossRef](#)] [[PubMed](#)]
6. Rossi, A.; Bellone, A.; Fokin, S.I.; Boscaro, V.; Vannini, C. Detecting Associations Between Ciliated Protists and Prokaryotes with Culture-Independent Single-Cell Microbiomics: A Proof-of-Concept Study. *Microb. Ecol.* **2019**, *78*, 232–242. [[CrossRef](#)] [[PubMed](#)]
7. Beale, G.H.; Jurand, A.; Preer, J.R. The Classes of Endosymbiont of *Paramecium aurelia*. *J. Cell Sci.* **1969**, *5*, 65–91. [[CrossRef](#)]
8. Preer, J.R.; Preer, L.B.; Jurand, A. Kappa and Other Endosymbionts in *Paramecium aurelia*. *Bacteriol. Rev.* **1974**, *38*, 113–163. [[CrossRef](#)]

9. Fujishima, M. (Ed.) *Endosymbionts in Paramecium*; Microbiology Monographs; Springer: Berlin/Heidelberg, Germany, 2009; Volume 12, ISBN 978-3-540-92676-4.
10. Fujishima, M.; Kodama, Y. Endosymbionts in *Paramecium*. *Eur. J. Protistol.* **2012**, *48*, 124–137. [[CrossRef](#)]
11. Lohse, K.; Gutierrez, A.; Kaltz, O. Experimental Evolution of Resistance in *Paramecium caudatum* against the Bacterial Parasite *Holospira undulata*. *Evolution* **2006**, *60*, 1177–1186.
12. Grosser, K.; Ramasamy, P.; Amirabad, A.D.; Schulz, M.H.; Gasparoni, G.; Simon, M.; Schrällhammer, M. More than the “Killer Trait”: Infection with the Bacterial Endosymbiont *Caedibacter taeniospiralis* Causes Transcriptomic Modulation in *Paramecium* Host. *Genome Biol. Evol.* **2018**, *10*, 646–656. [[CrossRef](#)]
13. Castelli, M.; Sabaneyeva, E.L.; Lanzoni, O.; Lebedeva, N.; Floriano, A.-M.; Gaiarsa, S.; Benken, K.; Modeo, L.; Bandi, C.; Potekhin, A.; et al. Deianiraea, an Extracellular Bacterium Associated with the Ciliate *Paramecium*, Suggests an Alternative Scenario for the Evolution of Rickettsiales. *ISME J.* **2019**, *13*, 2280–2294. [[CrossRef](#)] [[PubMed](#)]
14. Plotnikov, A.; Balkin, A.; Gogoleva, N.; Lanzoni, O.; Khlopko, Y.; Cherkasov, S.; Potekhin, A. High-Throughput Sequencing of the 16S rRNA Gene as a Survey to Analyze the Microbiomes of Free-Living Ciliates *Paramecium*. *Microb. Ecol.* **2019**, *78*, 286–298. [[CrossRef](#)] [[PubMed](#)]
15. Korotaev, A.; Benken, K.; Sabaneyeva, E. “*Candidatus* *Mystax nordicus*” Aggregates with Mitochondria of Its Host, the Ciliate *Paramecium nephridiatum*. *Diversity* **2020**, *12*, 251. [[CrossRef](#)]
16. Castelli, M.; Lanzoni, O.; Nardi, T.; Lometto, S.; Modeo, L.; Potekhin, A.; Sassera, D.; Petroni, G. ‘*Candidatus* *Sarmatiella mevalonica*’ Endosymbiont of the Ciliate *Paramecium* Provides Insights on Evolutionary Plasticity among Rickettsiales. *Environ. Microbiol.* **2021**, *23*, 1684–1701. [[CrossRef](#)] [[PubMed](#)]
17. Castelli, M.; Lanzoni, O.; Giovannini, M.; Lebedeva, N.; Gammuto, L.; Sassera, D.; Melekhin, M.; Potekhin, A.; Fokin, S.; Petroni, G. “*Candidatus* *Gromoviella Agglomerans*”, a Novel Intracellular *Holosporaceae* Parasite of the Ciliate *Paramecium* Showing Marked Genome Reduction. *Env. Environ. Microbiol. Rep.* **2022**, *14*, 34–49. [[CrossRef](#)]
18. Castelli, M.; Serra, V.; Senra, M.; Basuri, C.; Soares, C.; Fokin, S.; Modeo, L.; Petroni, G. The Hidden World of Rickettsiales Symbionts: “*Candidatus* *Spectrickettsia obscura*”, a Novel Bacterium Found in Brazilian and Indian *Paramecium caudatum*. *Microb. Ecol.* **2019**, *77*, 748–758. [[CrossRef](#)] [[PubMed](#)]
19. Schrällhammer, M.; Castelli, M.; Petroni, G. Phylogenetic Relationships among Endosymbiotic R-Body Producer: Bacteria Providing Their Host the Killer Trait. *Syst. Appl. Microbiol.* **2018**, *41*, 213–220. [[CrossRef](#)]
20. Szokoli, F.; Sabaneyeva, E.; Castelli, M.; Krenek, S.; Schrällhammer, M.; Soares, C.; da Silva-Neto, I.; Berendonk, T.; Petroni, G. “*Candidatus* *Fokinia solitaria*”, a Novel “Stand-alone” Symbiotic Lineage of *Midichloriaceae* (Rickettsiales). *PLoS ONE* **2016**, *11*, e0145743.
21. Lanzoni, O.; Sabaneyeva, E.; Modeo, L.; Castelli, M.; Lebedeva, N.V.; Verni, F.; Schrällhammer, M.; Potekhin, A.; Petroni, G. Diversity and Environmental Distribution of the Cosmopolitan Endosymbiont “*Candidatus* *Megaira*”. *Sci. Rep.* **2019**, *9*, 1179. [[CrossRef](#)]
22. Mironov, T.; Sabaneyeva, E. A Robust Symbiotic Relationship Between the Ciliate *Paramecium multimicronucleatum* and the Bacterium *Ca. Trichorickettsia mobilis*. *Front. Microbiol.* **2020**, *11*, 603335. [[CrossRef](#)]
23. Giannotti, D.; Boscaro, V.; Husnik, F.; Vannini, C.; Keeling, P.J. The “Other” Rickettsiales: An Overview of the Family “*Candidatus* *Midichloriaceae*”. *Appl. Environ. Microbiol.* **2022**, *88*, e02432-21. [[CrossRef](#)] [[PubMed](#)]
24. Thomas, S.; Alexander, W.; Gilligan, J.; Rikihisa, Y. The Importance of Rickettsiales Infections. In *Rickettsiales: Biology, Molecular Biology, Epidemiology, and Vaccine Development*; Thomas, S., Ed.; Springer International Publishing: Cham, Germany, 2016; pp. 3–21. ISBN 978-3-319-46859-4.
25. Boss, A.; Borkhansen, O.O.; Ossipov, D. *Pseudolyticum multiflagellatum* n. sp. a New Symbiotic Bacterium in the Cytoplasm of *Paramecium caudatum* (Ciliata, Protozoa). *Cytologia* **1987**, *29*, 94–99.
26. Preer, J.R.; Preer, L.B. Revival of Names of Protozoan Endosymbionts and Proposal of *Holospira caryophila* nom. nov. *Int. J. Syst. Bacteriol.* **1982**, *32*, 140–141. [[CrossRef](#)]
27. Fokin, S. Bacterial endobionts in the ciliate *Paramecium woodruffi*. III. Endobionts of the cytoplasm. *Cytologia* **1989**, *31*, 964–970.
28. Fokin, S.; Stoeck, T.S.; Schmidt, H.J. Rediscovery of *Paramecium nephridiatum* Gelei, 1925 and its Characteristics. *J. Eukaryot. Microbiol.* **1999**, *46*, 416–426. [[CrossRef](#)]
29. Fokin, S.I.; Görtz, H.-D. Diversity of *Holospira* Bacteria in *Paramecium* and Their Characterization. In *Endosymbionts in Paramecium*; Fujishima, M., Ed.; Microbiology Monographs; Springer: Berlin/Heidelberg, Germany, 2009; pp. 161–199. ISBN 978-3-540-92677-1.
30. Schweikert, M.; Fujishima, M.; Görtz, H.-D. Symbiotic Associations Between Ciliates and Prokaryotes. In *The Prokaryotes: Prokaryotic Biology and Symbiotic Associations*; Rosenberg, E., DeLong, E.F., Lory, S., Stackebrandt, E., Thompson, F., Eds.; Springer: Berlin/Heidelberg, Germany, 2013; pp. 427–463. ISBN 978-3-642-30194-0.
31. Sonneborn, T.M. Methods in *Paramecium* Research. In *Methods in Cell Biology*; Elsevier: Amsterdam, The Netherlands, 1970; Volume 4, pp. 241–339.
32. Fokin, S. *Paramecium* Genus: Biodiversity, Some Morphological Features and the Key to the Main Morphospecies Discrimination. *Protistology* **2010**, *6*, 227–235.
33. Medlin, L.; Elwood, H.; Stickel, S.S.; Sogin, M.L. The Characterization of Enzymatically Amplified Eukaryotic 16S-like rRNA-Coding Regions. *Gene* **1988**, *71*, 491–499. [[CrossRef](#)]
34. Petroni, G.; Dini, F.; Verni, F.; Rosati, G. A Molecular Approach to the Tangled Intrageneric Relationships Underlying Phylogeny in Euplotes (Ciliophora, Spirotrichea). *Mol. Phylogenetics Evol.* **2002**, *22*, 118–130. [[CrossRef](#)]

35. Rosati, G.; Modeo, L.; Melai, M.; Petroni, G.; Verni, F. A Multidisciplinary Approach to Describe Protists: A Morphological, Ultrastructural, and Molecular study on *Peritromus kahli* Villeneuve-Brachon, 1940 (Ciliophora, Heterotrichea). *J. Eukaryot. Microbiol.* **2004**, *51*, 49–59. [[CrossRef](#)]
36. Strueder-Kypke, M.L.; Lynn, D. Comparative Analysis of the Mitochondrial Cytochrome c Oxidase Subunit I (COI) Gene in Ciliates (Alveolata, Ciliophora) and Evaluation of Its Suitability as a Biodiversity Marker. *Syst. Biodivers.* **2010**, *8*, 131–148. [[CrossRef](#)]
37. Vannini, C.; Rosati, G.; Verni, F.; Petroni, G. Identification of the Bacterial Endosymbionts of the Marine Ciliate *Euplotes magnicirratu* (Ciliophora, Hypotrichia) and Proposal of “*Candidatus Devosia Euplotis*”. *Int. J. Syst. Evol. Microbiol.* **2004**, *54*, 1151–1156. [[CrossRef](#)] [[PubMed](#)]
38. Don, R.H.; Cox, P.T.; Wainwright, B.J.; Baker, K.; Mattick, J.S. ‘Touchdown’ PCR to Circumvent Spurious Priming during Gene Amplification. *Nucleic Acids Res.* **1991**, *19*, 4008. [[CrossRef](#)]
39. Ludwig, W.; Strunk, O.; Westram, R.; Richter, L.; Meier, H.; Yadukumar, Buchner, A.; Lai, T.; Steppi, S.; Jobb, G.; et al. ARB: A Software Environment for Sequence Data. *Nucleic Acids Res.* **2004**, *32*, 1363–1371. [[CrossRef](#)]
40. Quast, C.; Pruesse, E.; Yilmaz, P.; Gerken, J.; Schweer, T.; Yarza, P.; Peplies, J.; Glöckner, F.O. The SILVA Ribosomal RNA Gene Database Project: Improved Data Processing and Web-Based Tools. *Nucleic Acids Res.* **2013**, *41*, D590–D596. [[CrossRef](#)] [[PubMed](#)]
41. Cole, J.R.; Wang, Q.; Fish, J.A.; Chai, B.; McGarrell, D.M.; Sun, Y.; Brown, C.T.; Porras-Alfaro, A.; Kuske, C.R.; Tiedje, J.M. Ribosomal Database Project: Data and Tools for High Throughput RRNA Analysis. *Nucleic Acids Res.* **2014**, *42*, D633–D642. [[CrossRef](#)] [[PubMed](#)]
42. Greuter, D.; Loy, A.; Horn, M.; Rattei, T. ProbeBase—An Online Resource for RRNA-Targeted Oligonucleotide Probes and Primers: New Features 2016. *Nucleic Acids Res.* **2016**, *44*, D586–D589. [[CrossRef](#)] [[PubMed](#)]
43. Lindrea, K.C.; Seviour, E.M.; Seviour, R.J.; Blackall, L.L.; Soddell, J.A. Practical Methods for the Examination and Characterization of Activated Sludge. In *The Microbiology of Activated Sludge*; Seviour, R.J., Blackall, L.L., Eds.; Springer: Dordrecht, The Netherlands, 1998; pp. 257–300. ISBN 978-94-011-3951-9. [[CrossRef](#)]
44. Amann, R.I.; Binder, B.J.; Olson, R.J.; Chisholm, S.W.; Devereux, R.S.; Stahl, D. Combination of 16S RRNA-Targeted Oligonucleotide Probes with Flow Cytometry for Analyzing Mixed Microbial Populations. *Appl. Environ. Microbiol.* **1990**, *56*, 1919–1925. [[CrossRef](#)]
45. Manz, W.; Amann, R.; Ludwig, W.; Wagner, M.S.; Schleifer, K.-H. Phylogenetic Oligodeoxynucleotide Probes for the Major Subclasses of Proteobacteria: Problems and Solutions. *Syst. Appl. Microbiol.* **1992**, *15*, 593–600. [[CrossRef](#)]
46. Sayers, E.W.; Beck, J.; Bolton, E.E.; Bourexis, D.; Brister, J.R.; Canese, K.; Comeau, D.C.; Funk, K.; Kim, S.; Klimke, W.; et al. Database Resources of the National Center for Biotechnology Information. *Nucleic Acids Res.* **2020**, *49*, D10–D17. [[CrossRef](#)] [[PubMed](#)]
47. Johnson, M.; Zaretskaya, I.; Raytselis, Y.; Merezuk, Y.; McGinnis, S.; Madden, T.L. NCBI BLAST: A Better Web Interface. *Nucleic Acids Res.* **2008**, *36*, W5–W9. [[CrossRef](#)] [[PubMed](#)]
48. Katoh, K.; Standley, D.M. MAFFT Multiple Sequence Alignment Software Version 7: Improvements in Performance and Usability. *Mol. Biol. Evol.* **2013**, *30*, 772–780. [[CrossRef](#)] [[PubMed](#)]
49. Castresana, J. Selection of Conserved Blocks from Multiple Alignments for Their Use in Phylogenetic Analysis. *Mol. Biol. Evol.* **2000**, *17*, 540–552. [[CrossRef](#)]
50. Trifinopoulos, J.; Nguyen, L.-T.; von Haeseler, A.; Minh, B.Q. W-IQ-TREE: A Fast Online Phylogenetic Tool for Maximum Likelihood Analysis. *Nucleic Acids Res.* **2016**, *44*, W232–W235. [[CrossRef](#)] [[PubMed](#)]
51. Hoang, D.T.; Chernomor, O.; von Haeseler, A.; Minh, B.Q.; Vinh, L.S. UFBoot2: Improving the Ultrafast Bootstrap Approximation. *Mol. Biol. Evol.* **2018**, *35*, 518–522. [[CrossRef](#)]
52. Guindon, S.; Dufayard, J.-F.; Lefort, V.; Anisimova, M.; Hordijk, W.; Gascuel, O. New Algorithms and Methods to Estimate Maximum-Likelihood Phylogenies: Assessing the Performance of PhyML 3.0. *Syst. Biol.* **2010**, *59*, 307–321. [[CrossRef](#)] [[PubMed](#)]
53. Anisimova, M.; Gil, M.; Dufayard, J.-F.; Dessimoz, C.; Gascuel, O. Survey of Branch Support Methods Demonstrates Accuracy, Power, and Robustness of Fast Likelihood-Based Approximation Schemes. *Syst. Biol.* **2011**, *60*, 685–699. [[CrossRef](#)]
54. Letunic, I.; Bork, P. Interactive Tree Of Life (ITOL) v5: An Online Tool for Phylogenetic Tree Display and Annotation. *Nucleic Acids Res.* **2021**, *49*, W293–W296. [[CrossRef](#)]
55. BioRender. Available online: <https://www.biorender.com/> (accessed on 30 May 2023).
56. Inkscape. Available online: <https://inkscape.org> (accessed on 30 May 2023).
57. Dévényi, T.; Gergely, J. *Amino Acids, Peptides and Proteins: Biochemical and Immunochemical Techniques in Protein Chemistry*; Amsterdam; Elsevier Scientific Pub. Co.: New York, NY, USA, 1974; ISBN 978-0-444-41127-3.
58. Elghetany, M.T.; Saleem, A. Methods for Staining Amyloid in Tissues: A Review. *Stain. Technol.* **1988**, *63*, 201–212. [[CrossRef](#)]
59. Burdon, K.L. Fatty Material in Bacteria and Fungi Revealed by Staining Dried, Fixed Slide Preparations. *J. Bacteriol.* **1946**, *52*, 665–678. [[CrossRef](#)]
60. Strüder-Kypke, M.C.; Wright, A.D.; Fokin, S.I.; Lynn, D.H. Phylogenetic Relationships of the Subclass Peniculia (Oligohymenophorea, Ciliophora) Inferred from Small Subunit RRNA Gene Sequences. *J. Eukaryot. Microbiol.* **2000**, *47*, 419–429. [[CrossRef](#)]
61. Hoshina, R.; Hayashi, S.; Imamura, N. Intraspecific Genetic Divergence of *Paramecium bursaria* and Re-Construction of the Paramecian Phylogenetic Tree. *Acta Protozool.* **2006**, *45*, 377–386.
62. Fokin, S.I.; Lebedeva, N.A.; Potekhin, A.; Gammuto, L.; Petroni, G.; Serra, V. Holospora-like Bacteria “*Candidatus Gortzia yakutica*” and *Preeria caryophila*: Ultrastructure, Promiscuity, and Biogeography of the Symbionts. *Eur. J. Protistol.* **2023**, *90*, 125998. [[CrossRef](#)]
63. Barth, D.; Berendonk, T.U. The Mitochondrial Genome Sequence of the Ciliate *Paramecium caudatum* Reveals a Shift in Nucleotide Composition and Codon Usage within the Genus *Paramecium*. *BMC Genom.* **2011**, *12*, 272. [[CrossRef](#)] [[PubMed](#)]

64. Boscaro, V.; Husnik, F.; Vannini, C.; Keeling, P.J. Symbionts of the Ciliate *Euplotes*: Diversity, Patterns and Potential as Models for Bacteria–Eukaryote Endosymbioses. *Proc. Biol. Sci.* **2019**, *286*, 20190693. [[CrossRef](#)]
65. Szokoli, F.; Castelli, M.; Sabaneyeva, E.; Schrallhammer, M.; Krenek, S.; Doak, T.G.; Berendonk, T.U.; Petroni, G. Disentangling the Taxonomy of Rickettsiales and Description of Two Novel Symbionts (“*Candidatus* Bealeia paramacronuclearis” and “*Candidatus* Fokinia cryptica”) Sharing the Cytoplasm of the Ciliate Protist *Paramecium biaurelia*. *Appl. Environ. Microbiol.* **2016**, *82*, 7236–7247. [[CrossRef](#)] [[PubMed](#)]
66. Boscaro, V.; Petroni, G.; Ristori, A.; Verni, F.; Vannini, C. “*Candidatus* Defluviella procrastinata” and “*Candidatus* Cyrtobacter zanobii”, Two Novel Ciliate Endosymbionts Belonging to the “Midichloria Clade”. *Microb. Ecol.* **2013**, *65*, 302–310. [[CrossRef](#)]
67. Yarza, P.; Yilmaz, P.; Pruesse, E.; Glöckner, F.O.; Ludwig, W.; Schleifer, K.-H.; Whitman, W.B.; Euzéby, J.; Amann, R.; Rosselló-Móra, R. Uniting the Classification of Cultured and Uncultured Bacteria and Archaea Using 16S rRNA Gene Sequences. *Nat. Rev. Microbiol.* **2014**, *12*, 635–645. [[CrossRef](#)]
68. Karasz, D.C.; Weaver, A.I.; Buckley, D.H.; Wilhelm, R.C. Conditional Filamentation as an Adaptive Trait of Bacteria and Its Ecological Significance in Soils. *Environ. Microbiol.* **2022**, *24*, 1–17. [[CrossRef](#)] [[PubMed](#)]
69. van Teeseling, M.C.F.; de Pedro, M.A.; Cava, F. Determinants of Bacterial Morphology: From Fundamentals to Possibilities for Antimicrobial Targeting. *Front. Microbiol.* **2017**, *8*, 1264. [[CrossRef](#)] [[PubMed](#)]
70. Corno, G.; Jürgens, K. Direct and Indirect Effects of Protist Predation on Population Size Structure of a Bacterial Strain with High Phenotypic Plasticity. *Appl. Environ. Microbiol.* **2006**, *72*, 78–86. [[CrossRef](#)] [[PubMed](#)]
71. Tran, T.D.; Ali, M.A.; Lee, D.; Félix, M.-A.; Luallen, R.J. Bacterial Filamentation as a Mechanism for Cell-to-Cell Spread within an Animal Host. *Nat. Commun.* **2022**, *13*, 693. [[CrossRef](#)]
72. Boscaro, V.; Schrallhammer, M.B.; Benken, K.A.; Krenek, S.; Szokoli, F.; Berendonk, T.U.; Schweikert, M.; Verni, F.; Sabaneyeva, E.V.; Petroni, G. Rediscovering the Genus *Lyticum*, Multiflagellated Symbionts of the Order Rickettsiales. *Sci. Rep.* **2013**, *3*, 3305. [[CrossRef](#)] [[PubMed](#)]
73. Neubauer, P.; Fahnert, B.; Lilie, H.; Villaverde, A. Protein Inclusion Bodies in Recombinant Bacteria. In *Inclusions in Prokaryotes*; Shively, J.M., Ed.; Microbiology Monographs; Springer: Berlin/Heidelberg, Germany, 2006; pp. 237–292. ISBN 978-3-540-33774-4.
74. Park, H.-W.; Federici, B.A.; Sakano, Y. Inclusion Proteins from Other Insecticidal Bacteria. In *Inclusions in Prokaryotes*; Shively, J.M., Ed.; Microbiology Monographs; Springer: Berlin/Heidelberg, Germany, 2006; pp. 321–330. ISBN 978-3-540-33774-4.
75. Pötter, M.; Steinbüchel, A. Biogenesis and Structure of Polyhydroxyalkanoate Granules. In *Inclusions in Prokaryotes*; Shively, J.M., Ed.; Microbiology Monographs; Springer: Berlin/Heidelberg, Germany, 2006; pp. 109–136. ISBN 978-3-540-33774-4.
76. Wältermann, M.; Steinbüchel, A. Wax Ester and Triacylglycerol Inclusions. In *Inclusions in Prokaryotes*; Shively, J.M., Ed.; Microbiology Monographs; Springer: Berlin/Heidelberg, Germany, 2006; pp. 137–166. ISBN 978-3-540-33774-4.
77. Schrallhammer, M.; Schweikert, M. The Killer Effect of *Paramecium* and Its Causative Agents. In *Endosymbionts in Paramecium*; Fujishima, M., Ed.; Microbiology Monographs; Springer: Berlin/Heidelberg, Germany, 2009; pp. 227–246. ISBN 978-3-540-92677-1.
78. Pond, F.R.; Gibson, I.; Lalucat, J.; Quackenbush, R.L. R-Body-Producing Bacteria. *Microbiol. Rev.* **1989**, *53*, 25–67. [[CrossRef](#)] [[PubMed](#)]
79. Sanchez-Amat, A. R-Bodies. In *Inclusions in Prokaryotes*; Shively, J.M., Ed.; Microbiology Monographs; Springer: Berlin/Heidelberg, Germany, 2006; pp. 331–341. ISBN 978-3-540-33774-4.
80. Wang, B.; Lin, Y.-C.; Vasquez-Rifo, A.; Jo, J.; Price-Whelan, A.; McDonald, S.T.; Brown, L.M.; Sieben, C.; Dietrich, L.E.P. *Pseudomonas aeruginosa* PA14 Produces R-Bodies, Extendable Protein Polymers with Roles in Host Colonization and Virulence. *Nat. Commun.* **2021**, *12*, 4613. [[CrossRef](#)] [[PubMed](#)]
81. Fiebig, A.; Pradella, S.; Petersen, J.; Päuker, O.; Michael, V.; Lünsdorf, H.; Göker, M.; Klenk, H.-P.; Wagner-Döbler, I. Genome of the R-Body Producing Marine Alphaproteobacterium *Labrenzia alexandrii* Type Strain (DFL-11T). *Stand. Genom. Sci.* **2013**, *7*, 413–426. [[CrossRef](#)] [[PubMed](#)]
82. Matsuoka, J.; Ishizuna, F.; Kurumisawa, K.; Morohashi, K.; Ogawa, T.; Hidaka, M.; Saito, K.; Ezawa, T.; Aono, T. Stringent Expression Control of Pathogenic R-Body Production in Legume Symbiont *Azorhizobium caulinodans*. *mBio* **2017**, *8*, e00715-17. [[CrossRef](#)] [[PubMed](#)]
83. Raymann, K.; Bobay, L.-M.; Doak, T.G.; Lynch, M.; Gribaldo, S. A Genomic Survey of Reb Homologs Suggests Widespread Occurrence of R-Bodies in Proteobacteria. *G3 Genes Genomes Genet.* **2013**, *3*, 505–516. [[CrossRef](#)] [[PubMed](#)]
84. Federici, B.A.; Lüthy, P.; Ibarra, J.E. Parasporal Body of *Bacillus thuringiensis israelensis*. In *Bacterial Control of Mosquitoes & Black Flies: Biochemistry, Genetics & Applications of Bacillus Thuringiensis israelensis and Bacillus sphaericus*; de Barjac, H., Sutherland, D.J., Eds.; Springer: Dordrecht, The Netherlands, 1990; pp. 16–44. ISBN 978-94-011-5967-8.
85. Schönherr, R.; Rudolph, J.M.; Redecke, L. Protein Crystallization in Living Cells. *Biol. Chem.* **2018**, *399*, 751–772. [[CrossRef](#)]
86. Glare, T.R.; Jurat-Fuentes, J.-L.; O’Callaghan, M. Chapter 4—Basic and Applied Research: Entomopathogenic Bacteria. In *Microbial Control of Insect and Mite Pests*; Lacey, L.A., Ed.; Academic Press: Cambridge, MA, USA, 2017; pp. 47–67. ISBN 978-0-12-803527-6.
87. Cao, B.; Nie, Y.; Guan, Z.; Chen, C.; Wang, N.; Wang, Z.; Shu, C.; Zhang, J.; Zhang, D. The Crystal Structure of Cry78Aa from *Bacillus Thuringiensis* Provides Insights into Its Insecticidal Activity. *Commun. Biol.* **2022**, *5*, 801. [[CrossRef](#)] [[PubMed](#)]
88. Bowen, D.J.; Ensign, J.C. Isolation and Characterization of Intracellular Protein Inclusions Produced by the Entomopathogenic Bacterium *Photobacterium luminescens*. *Appl. Env. Environ. Microbiol.* **2001**, *67*, 4834–4841. [[CrossRef](#)]
89. You, J.; Liang, S.; Cao, L.; Liu, X.; Han, R. Nutritive Significance of Crystalline Inclusion Proteins of *Photobacterium luminescens* in *Steinernema* Nematodes. *FEMS Microbiol. Ecol.* **2006**, *55*, 178–185. [[CrossRef](#)] [[PubMed](#)]

90. Fokin, S.I.; Boss, A.O.-L.; Ossipov, D.V. A virus-containing cytoplasmic symbiont of the ciliate *Paramecium woodruffi*. *Tsitologiya* **1987**, *29*, 1303–1306.
91. Fokin, S.; Sabaneyeva, E. Bacterial Endocytobionts of the Ciliate *Paramecium calkinsi*. *Eur. J. Protistol.* **1993**, *29*, 390–395. [[CrossRef](#)] [[PubMed](#)]
92. Fokin, S.I.; Giamberini, L.; Molloy, D.P.; de Vaate, A.B. Bacterial Endocytobionts within Endosymbiotic Ciliates in *Dreissena polymorpha* (Lamellibranchia: Mollusca). *Acta Protozool.* **2003**, *42*, 31–40.
93. Berezina, I.G. An Electron Microscope Study of Endosymbionts in *Blepharisma japonicum*. *Acta Protozool.* **1974**, *13*, 365–369.
94. Fokin, S.I.; Schweikert, M. Bacterial Endocytobionts in the Macronucleus of *Frontonia leucas* (Ciliophora, Peniculida). *Eur. J. Protistol.* **2003**, *39*, 311–318. [[CrossRef](#)]
95. George, E.E.; Barcytè, D.; Lax, G.; Livingston, S.; Tashyreva, D.; Husnik, F.; Lukeš, J.; Eliáš, M.; Keeling, P.J. A Single Cryptomonad Cell Harbors a Complex Community of Organelles, Bacteria, a Phage, and Selfish Elements. *Curr. Biol.* **2023**, *33*, 1982–1996.e4. [[CrossRef](#)]

Disclaimer/Publisher’s Note: The statements, opinions and data contained in all publications are solely those of the individual author(s) and contributor(s) and not of MDPI and/or the editor(s). MDPI and/or the editor(s) disclaim responsibility for any injury to people or property resulting from any ideas, methods, instructions or products referred to in the content.